Cosmic crystallography: the hyperbolic isometries

A.F.F. Teixeira *
Centro Brasileiro de Pesquisas Físicas
22290-180 Rio de Janeiro-RJ, Brazil

November 22, 2000

Abstract

All orientation preserving isometries of the hyperbolic three-space are studied, and the probability density of conjugate pair separations for each isometry is presented. The study is relevant for the cosmic crystallography, and is the theoretical counterpart of the mean histograms arising from computer simulations of the isometries.

1 Introduction

Cosmic crystallography is a method to help finding the geometry and the topology of the universe [1]. In a close analysis of the method, a description has been presented of how each isometry of the universe gives its individual contribution to a pair separation histogram (PSH) [2]. More recently, the isometries of the infinite 3D *euclidean* space were studied in some detail, and the expected (theoretical) individual contribution of each isometry to the PSH was described [3].

The present report investigates the orientation preserving isometries of H^3, the 3D infinite *hyperbolic* space with positive definite metric and unitary radius of negative curvature. To generalize for arbitrary negative curvature one simply needs dividing every quantity with dimension length by the radius of curvature. All the results obtained clearly reproduce their euclidean counterparts when the radius of curvature tends to infinity.

2 The probability density of conjugate pair separations

In H^3 we assume a spherical solid ball $\mathcal{B}$. Under an isometry g of H^3 the ball occupies a new position $\mathcal{B}_g$; we only consider isometries such that the balls $\mathcal{B}$ and $\mathcal{B}_g$ intersect. Assuming a point $P \in \mathcal{B}$ and denoting as $P_g \in \mathcal{B}_g$ its g-transported, we call the pair (P, P_g) a g-pair. We focus our attention on the g-pairs such that $P_g \in \mathcal{B} \cap \mathcal{B}_g$, and assume an infinity of points P_g uniformly distributed throughout the intersection $\mathcal{B} \cap \mathcal{B}_g$. For the given isometry g, we ask for the probability $\mathcal{P}_g^{\mathcal{B}}(l)dl$ that a randomly selected g-pair has hyperbolic separation lying between the values l and $l + dl$; the probability density $\mathcal{P}_g^{\mathcal{B}}(l)$ clearly satisfies the normalization condition

$$\int_0^{2a} \mathcal{P}_g^{\mathcal{B}}(l)dl = 1, \tag{1}$$

where $2a$ is the diametre of the balls.

3 Some basic formulas

A few useful formulas of the hyperbolic trigonometry in 2D are worth having at hand. In a geodetic triangle with sides measuring a, b, c and corresponding opposite angles measuring α, β, γ, we have

- the law of sines

$$\frac{\sin\alpha}{\sinh a} = \frac{\sin\beta}{\sinh b} = \frac{\sin\gamma}{\sinh c}; \tag{2}$$

- the first law of cosines (cyclic)

$$\begin{aligned}\cosh a = &\cosh b \cosh c \\ &- \sinh b \sinh c \cos\alpha \quad ;\end{aligned} \tag{3}$$

- the second law of cosines (cyclic)

$$\begin{aligned}\cos\alpha = &-(\cos\beta\cos\gamma \\ &- \sin\beta\sin\gamma\cosh a) \quad .\end{aligned} \tag{4}$$

We also need a few 2D relations between lengths of arcs of geodesics, horocycles and equidistant curves to a geodesic; see figure 1 for visualization:

$$\begin{aligned} e' = g\cosh r, \quad & h' = h\cosh r, \\ h = 2\sinh(g/2), \quad & e^f = \cosh(g/2), \\ \tanh p' = \tanh p \cosh q, & \end{aligned} \tag{5}$$

and as a consequence

$$\sinh(g'/2) = \sinh(g/2)\cosh r\,. \tag{6}$$

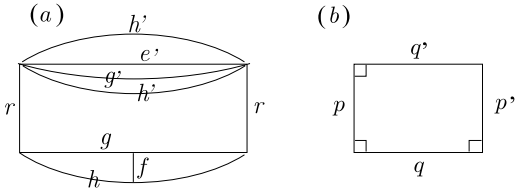

Figure 1 Some geometric objects in the plane hyperbolic geometry.

*teixeira@cbpf.br

(a) g, g', and r are geodetic arcs; h and h' are arcs of horocycles; e' is an arc equidistant to g; the arcs r are perpendicular to g and to e'; the geodetic arc f is orthogonal to both g and h.
(b) a geodetic quadrilateral with three right angles, assuming $\sinh p \sinh q < 1$.

We often use the line element of H^3 in the cylindrical coordinates,

$$dl^2 = d\rho^2 + \sinh^2\rho\, d\phi^2 + \cosh^2\rho\, d\zeta^2 ; \tag{7}$$

we also use

$$\begin{aligned} dl^2 &= -dW^2 + dX^2 + dY^2 + dZ^2 , \\ W &= \sqrt{1 + X^2 + Y^2 + Z^2} , \end{aligned} \tag{8}$$

where

$$\begin{aligned} W &= \cosh\rho\cosh\zeta , \quad X = \sinh\rho\cos\phi , \\ Y &= \sinh\rho\sin\phi , \quad Z = \cosh\rho\sinh\zeta \ . \end{aligned} \tag{9}$$

In these coordinates the separation l between two points P_1, P_2 is given by

$$\begin{aligned} \cosh l &= W_1W_2 - (X_1X_2 + Y_1Y_2 + Z_1Z_2) \\ &= \cosh\rho_1\cosh\rho_2\cosh(\zeta_1 - \zeta_2) \\ &\quad - \sinh\rho_1\sinh\rho_2\cos(\phi_1 - \phi_2) \ . \end{aligned} \tag{10}$$

For future reference, consider the special situation of the three points (see figure 2)

$$\begin{aligned} P_1 &= (\rho_1, 0, 0) = && (\cosh\rho_1; \sinh\rho_1, 0, 0) , \\ Q &= (0, 0, g) = && (\cosh g; 0, 0, \sinh g) , \\ P_2 &= (\rho_2, \phi, g) = && (\cosh\rho_2\cosh g; \sinh\rho_2\cos\phi , \\ & && \sinh\rho_2\sin\phi, \cosh\rho_2\sinh g) \ ; \end{aligned}$$

the separation l between the points P_1 and P_2 is then given by (10), namely

$$\begin{aligned} \cosh l = \ & \cosh\rho_1\cosh\rho_2\cosh g \\ & - \sinh\rho_1\sinh\rho_2\cos\phi \quad . \end{aligned} \tag{11}$$

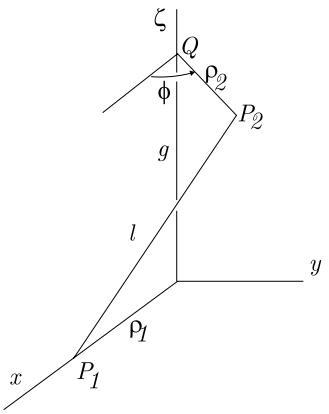

Figure 2 Relative position of points P_1 and P_2 with hyperbolic separation l.

4 The isometries of H^3

We are presently interested in the isometries of H^3 that preserve the orientation. These isometries can be classified as

- hyperbolic, with 5 parametres; these isometries bear some similarity with the 3-parametric euclidean translations;
- elliptic, also with 5 parametres; they are analogous to the also 5-parametric euclidean rotations in ordinary space;
- screw motions, with 6 parametres; bear some similarity with the also 6-parametric euclidean screw motions;
- parabolic, with only 4 parametres; again they remind us of the euclidean translations.

In each of these isometries the intersection of the balls $\mathcal{B}$ and $\mathcal{B}_g$ is a rotationally symmetric solid lens, whose thickness T, diametre $D = 2R$, and volume $V_g^{\mathcal{B}}$ we now seek. We denote as a the radius of the balls, and $m = 2M$ the separation between their centres C and C_g; then we clearly have $M < a$ and (see figure 3)

$$T = 2(a - M) . \tag{12}$$

The separation m depends on the isometry g one is concerned with. Noting that a, M, and R make a right-angled triangle with hypotenuse a, we find

$$\cosh a = \cosh M \cosh R . \tag{13}$$

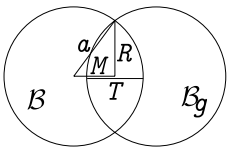

Figure 3 The balls $\mathcal{B}$ and $\mathcal{B}_g$ with radius a intersect in a solid lens with equatorial radius R and thickness T. The centres of the balls are separated $m = 2M$.

To have the volume $V_g^{\mathcal{B}}$ of the solid lens $\mathcal{B} \cap \mathcal{B}_g$ we first consider a compact cylindrical surface $\mathcal{C}_y$ embeded in the lens, and whose axis coincides with that of the lens (see figure 4); all points of $\mathcal{C}_y$ are at a fixed distance y from the axis, so the geometry on $\mathcal{C}_y$ is 2D-euclidean. Denoting as e the length of the generatrices (arcs equidistant to the geodetic axis), the area of $\mathcal{C}_y$ is

$$S(y) = 2\pi e \sinh y . \tag{14}$$

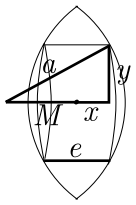

Figure 4 Sketch of a compact cylinder $\mathcal{C}_y$ inscribed in the solid lens $\mathcal{B}\cap\mathcal{B}_g$; it has radius y and generatrices e.

We must now relate e with a, M, and the variable radius y. In figure 4 we note a right angled triangle with sides a (hypotenuse), y, and $M+x$, so we have

$$\cosh a = \cosh y \cosh(M+x)\,; \tag{15}$$

since from eq. (5a) we have $e/2 = x\cosh y$, then $e = 2\cosh y\left[\cosh^{-1}\left(\frac{\cosh a}{\cosh y}\right) - M\right]$, and

$$S(y) = 2\pi\sinh 2y\left[\cosh^{-1}\left(\frac{\cosh a}{\cosh y}\right) - M\right]\,. \tag{16}$$

The volume $V_g^{\mathcal{B}}$ of the lens is clearly

$$V_g^{\mathcal{B}} = \int_0^R S(y)dy \tag{17}$$
$$= 2\pi\left[(\tanh a - \tanh M)\cosh^2 a - (a-M)\right]\,.$$

It can be checked that when $M=0$ we get the hyperbolic volume $\pi(\sinh 2a - 2a)$ of a solid ball with radius a, as expected. Also note that for small values of a and M we recover the euclidean volume $(2\pi/3)(a-M)^2(2a+M)$ of the solid lens [3] .

5 Special translations

Preceding the study of the *general hyperbolic* isometry of H^3 we first consider the very special situation in which the axis $\mathcal{L}$ of the isometry g crosses the centre C of the ball $\mathcal{B}$. With a = the radius of $\mathcal{B}$, and t = the value of the translation along the axis, we assume $t<2a$ to have nonvanishing intersection $\mathcal{B}\cap\mathcal{B}_g$. In this special isometry we clearly have the equality $m=t$.

According to eq.(6) and figure 1, a point P at a distance r from the axis $\mathcal{L}$ is displaced under t to a distance l given by

$$\sinh(l/2) = \sinh(t/2)\cosh r\,; \tag{18}$$

this is a relation involving the variable l (displacement of P), the variable r (distance from P to the axis $\mathcal{L}$), and the parametre t (the unique relevant one in this special isometry).

We next introduce the probability $Q_g^{\mathcal{B}}(r)dr$ that a randomly chosen point P_g which is in both $\mathcal{B}$ and $\mathcal{B}_g$ be in a radial position between r and $r+dr$. The probability density $Q_g^{\mathcal{B}}(r)$ clearly is proportional to the area $S_g^{\mathcal{B}}(r)$ of the cylinder $\mathcal{C}_r$ inscribed in the solid lens $\mathcal{B}\cap\mathcal{B}_g$ (see eq.(16)), the coefficient of proportionality being the inverse of the volume $V_g^{\mathcal{B}}$ of the lens:

$$Q_g^{\mathcal{B}}(r) = \frac{S_g^{\mathcal{B}}(r)}{V_g^{\mathcal{B}}}$$
$$= \frac{2\pi}{V_g^{\mathcal{B}}}\sinh 2r\left[\cosh^{-1}\left(\frac{\cosh a}{\cosh r}\right) - \frac{t}{2}\right]\,. \tag{19}$$

The equality of the probabilities $\mathcal{P}_g^{\mathcal{B}}(l)dl$ and $Q_g^{\mathcal{B}}(r)dr$ then gives, using $r(l)$ obtained from (18),

$$\mathcal{P}_g^{\mathcal{B}}(l) = \frac{dr}{dl}Q_g^{\mathcal{B}}[r(l)] \tag{20}$$
$$= \frac{1}{V_g^{\mathcal{B}}}\frac{\pi\sinh l}{\sinh^2 t/2}\left[\cosh^{-1}\left(\frac{\cosh a\sinh t/2}{\sinh l/2}\right) - \frac{t}{2}\right]\,.$$

In the figure 5 we have four instances of $\mathcal{P}_g^{\mathcal{B}}(l)$. Each plot starts abruptly on $l=t$ and vanishes when $\sinh(l/2) = \cosh a\tanh(t/2)$. They greatly differ from that of an euclidean translation, where $\mathcal{P}_g^{\mathcal{B}}(l) = \delta(l-t)$, a Dirac δ.

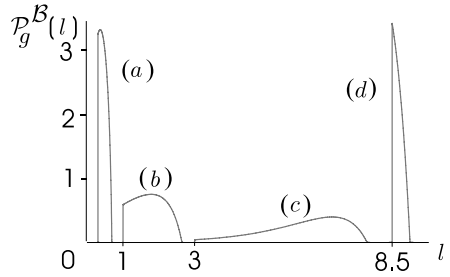

Figure 5 Probability densities $\mathcal{P}_g^{\mathcal{B}}(l)$ of pair separations for hyperbolic motions t of a ball $\mathcal{B}$ with radius a, when the axis of the isometry crosses the centre of the ball. In (a) we took $t=0.3$ and $a=1.5$; in (b), $t=1$ and $a=2$; in (c), $t=3$ and $a=4$; and in (d), $t=8.5$ and $a=4.5$. Plots (a) and (d) loosely resemble a Dirac δ mainly because the corresponding solid lenses $\mathcal{B}\cap\mathcal{B}_g$ have volume $V_g^{\mathcal{B}}$ small in comparison with the volume $\pi(\sinh 2a - 2a)$ of $\mathcal{B}$. All integrated areas are unitary.

6 Special screw motions

It is very simple to generalize the probability density (20) to further have a rotation ω of $\mathcal{B}$ around the axis $\mathcal{L}$ of the translation. See figure 6.

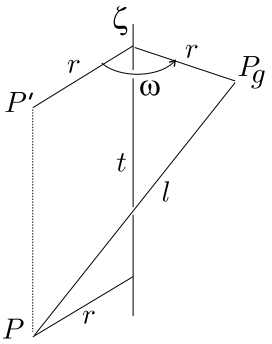

Figure 6 A screw motion of H^3 with axis along the ζ axis. Under the preliminary hyperbolic motion t (measured on the ζ axis) a point P is displaced to the intermediate position P'; then the rotation ω around ζ brings P' to the final position P_g geodetically separated l from P.

The separation l between a point P and the corresponding P_g is now given by (11), where we replace $\rho_1=\rho_2\to r$, $g\to t$, $\phi\to\omega$:

$$\cosh l = \cosh^2 r\cosh t - \sinh^2 r\cos\omega\,. \tag{21}$$

For fixed t and ω this gives $r(l)$, from which we derive dr/dl. Since neither the volume $V_g^{\mathcal{B}}$ nor the areas $S_g^{\mathcal{B}}(r)$ depend on ω in this special screw motion of $\mathcal{B}$, the density $Q_g^{\mathcal{B}}(r)$ is again given by (19). The density $\mathcal{P}_g^{\mathcal{B}}(l)$ is then

$$\mathcal{P}_g^{\mathcal{B}}(l) = \frac{2\pi \sinh l}{V_g^{\mathcal{B}}(\cosh t - \cos\omega)} \times \left[\cosh^{-1}\left(\cosh a \sqrt{\frac{\cosh t - \cos\omega}{\cosh l - \cos\omega}}\right) - \frac{t}{2}\right], \quad (22)$$

with $V_g^{\mathcal{B}}$ as given in (18) with $M = t/2$. A few sample plots of $\mathcal{P}_g^{\mathcal{B}}(l)$ are given in figure 7.

We clearly recover the equation (20) when $\omega = 0$. On the other hand, setting $t = 0$ in (22) gives the $\mathcal{P}_g^{\mathcal{B}}(l)$ for a special elliptic isometry, namely a pure rotation ω of the ball $\mathcal{B}$ when the axis of the rotation contains the centre of the ball:

$$\mathcal{P}_g^{\mathcal{B}}(l) = \frac{\pi \sinh l}{V_g^{\mathcal{B}} \sin^2(\omega/2)} \times \cosh^{-1}\left(\frac{\cosh a \sinh(\omega/2)}{\sqrt{\sinh^2(l/2) - \sinh^2(\omega/2)}}\right); \quad (23)$$

a special $\mathcal{P}_g^{\mathcal{B}}(l)$ with $t = 0$ is in figure 7(a).

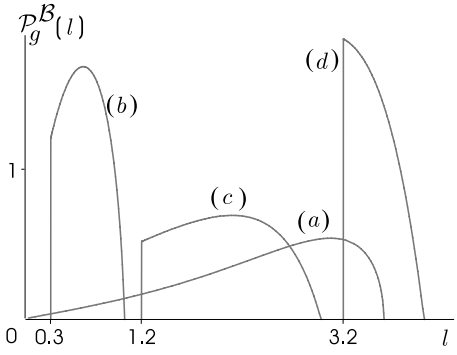

Figure 7 Probability densities $\mathcal{P}_g^{\mathcal{B}}(l)$ of pair separations for special screw motions $g = (t, \omega)$ of a ball $\mathcal{B}$ with radius a, when the axis of the isometry crosses the centre of the ball. In (a) we took $t = 0$ (no translation), $a = 1.8$, and $\omega = \pi$; in (b), $t = 0.3$, $a = 1.5$, and $\omega = \pi/8$; in (c), $t = 1.2$, $a = 2.0$, and $\omega = \pi/8$; and in (d), $t = 3.2$, $a = 2.0$, and $\omega = \pi$. Each plot starts at $l = t$, and abruptly except when we have pure rotation ($t = 0$, case (a)). All plots end when $\cosh l = \cosh^2\rho \cosh t - \sinh^2\rho \cos\omega$, with $\cosh\rho = \cosh a \ \mathrm{sech}(t/2)$. All integrated areas are unitary.

7 Parabolic motions

To describe a *parabolic* isometry g of H^3 we need first announce its 2-parametric apex A, a point at infinity. Next we select an arbitrary point C of H^3, and draw the unique horosphere $\mathcal{C}$ with centre A and containing C. Then, starting from C we mark an arc of horocycle with length μ, laying on $\mathcal{C}$; the direction of the arc and the value of μ demand two new parametres and finally fix the isometry g. The horocyclic separation between C and its g-transported C_g being μ, the corresponding geodetic separation m is given by eq.$(5c)$:

$$\mu = 2\sinh(m/2)\,. \quad (24)$$

We now consider a solid ball $\mathcal{B}$ with radius a and centre C; clearly there is no loss of generality in this last choice. The two parametres (a, m) suffice to completely describe $\mathcal{P}_g^{\mathcal{B}}(l)$.

Denote as r the geodetic altitude of a point P of H^3 relative to the horosphere $\mathcal{C}$; r is counted positive if P is outside $\mathcal{C}$, and negative if inside. Also draw the horosphere $\mathcal{C}_r$ with apex A and intersecting P. Under the isometry g all points of $\mathcal{C}_r$ are equally displaced along horocyclic arcs laying on $\mathcal{C}_r$, and measuring

$$\lambda = \mu\, e^r\,; \quad (25)$$

equivalently, the geodetic separation l between P and P_g is given by (see figure 8)

$$\sinh(l/2) = e^r \sinh(m/2)\,. \quad (26)$$

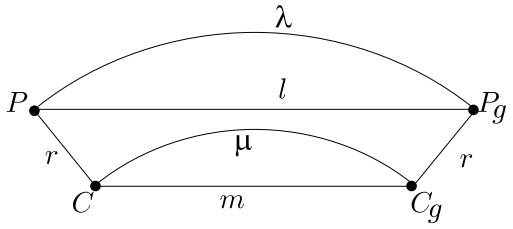

Figure 8 A parabolic isometry g of H^3 brings the points C and P to C_g and P_g, respectively; m and l are geodetic arcs, μ and λ are horocyclic arcs; r are parallel geodetic arcs orthogonal to both μ and λ; all arcs lay in a same H^2.

For future use we compute dr/dl from (26), with m fixed:

$$\frac{dr}{dl} = \frac{1}{2}\coth(\frac{l}{2})\,. \quad (27)$$

The horosphere $\mathcal{C}_r$ intersects each solid ball $\mathcal{B}$ and $\mathcal{B}_g$ in flat circular disks $\mathcal{D}_r$ and $\mathcal{D}_{rg}$, both with radius ρ. To have ρ as a function of r and a we introduce an auxiliary variable s (see figure 9) and solve the system

$$\cosh a = \cosh s \cosh(r - f)\,, \qquad e^f = \cosh s\,, \qquad \rho = \sinh s\,, \quad (28)$$

which gives

$$\rho = \sqrt{2(\cosh a - \cosh r)e^r}\,. \quad (29)$$

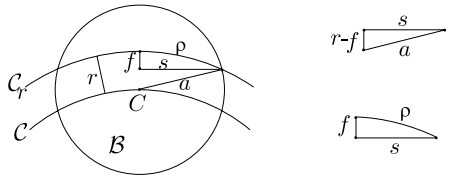

Figure 9 $\mathcal{C}_r$ and $\mathcal{C}$ are equidistant horospheres both intersecting the solid ball $\mathcal{B}$ with centre C and radius a. We note a right-angled geodetic triangle with sides a (hypotenuse),

s, and $r-f$, where f is the geodetic arc orthogonal to both the geodetic arc s and the horocyclic arc ρ.

Our geometric situation is now phrased in the following terms: in a 2D flat plane (the horosphere $\mathcal{C}_r$) we have two circular disks $\mathcal{D}_r$ and $\mathcal{D}_{rg}$, both with radius ρ, whose centres are separated by λ. We ask for the probability $R_g^{\mathcal{B}}(r)dr$ that a randomly chosen g-pair (P, P_g), such that $P_g \in \mathcal{B}\cap\mathcal{B}_g$, has altitude between r and $r+dr$. Clearly the probability density $R_g^{\mathcal{B}}(r)$ is proportional to the area $S_g^{\mathcal{B}}(r)$ of the intersection $\mathcal{D}_r \cap \mathcal{D}_{rg}$, the coefficient of proportionality being the inverse of the volume $V_g^{\mathcal{B}}$ of the solid lens $\mathcal{B}\cap\mathcal{B}_g$:

$$R_g^{\mathcal{B}}(r) = \frac{S_g^{\mathcal{B}}(r)}{V_g^{\mathcal{B}}}\,. \tag{30}$$

The euclidean area $S_g^{\mathcal{B}}(r)$ is simple to obtain (see figure 10), it is

$$S_g^{\mathcal{B}}(r) = 4\left[\frac{1}{2}\alpha\rho^2 - \frac{\lambda}{4}\sqrt{\rho^2-\lambda^2/4}\right] \tag{31}$$

with $\lambda = 2\sinh(l/2)$, $\rho(r)$ as in (29), and $\cos\alpha(r) = \lambda/(2\rho)$.

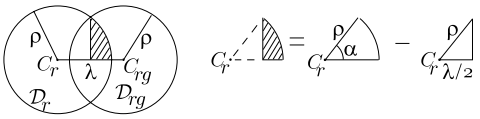

Figure 10 $\mathcal{D}_r$ and $\mathcal{D}_{rg}$ are coplanar flat circular disks with radius ρ and with separation λ between their centres C_r and C_{rg}. The area $S_g^{\mathcal{B}}(r)$ of the intersection $\mathcal{D}_r \cap \mathcal{D}_{rg}$ is four times the shadowed area.

Since the probabilities $\mathcal{P}_g^{\mathcal{B}}(l)dl$ and $R_g^{\mathcal{B}}(r)dr$ are the same, we finally have

$$\begin{aligned}\mathcal{P}_g^{\mathcal{B}}(l) &= \frac{dr}{dl}R_g^{\mathcal{B}}[r(l)] = \frac{dr}{dl}\frac{S_g^{\mathcal{B}}[r(l)]}{V_g^{\mathcal{B}}} \\ &= \frac{\coth(l/2)}{V_g^{\mathcal{B}}}\left[\rho^2\cos^{-1}\left(\frac{\sinh(l/2)}{\rho}\right)\right. \\ &\quad \left. -\sinh(l/2)\sqrt{\rho^2-\sinh^2(l/2)}\right],\end{aligned} \tag{32}$$

with $\rho(l) =$

$$\sqrt{\sinh^2 a - [\cosh a - \sinh(l/2)/\sinh(m/2)]^2}\,. \tag{33}$$

See figure 11, where examples of $\mathcal{P}_g^{\mathcal{B}}(l)$ for parabolic isometries are reproduced. In each plot we have l_{max} and l_{min} given respectively by $\sinh(l/2) = \tanh(m/2)e^{\pm R}$, with $\cosh R = \cosh a\ \mathrm{sech}(m/2)$.

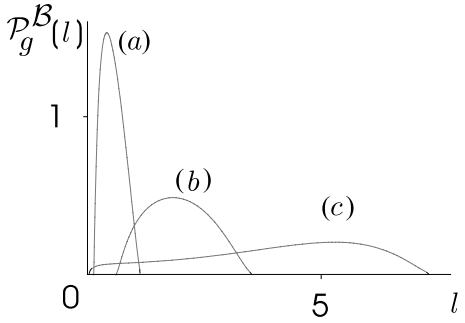

Figure 11 Probability densities $\mathcal{P}_g^{\mathcal{B}}(l)$ of pair separations for parabolic isometries g of a solid ball $\mathcal{B}$ with radius a. Under g, the centre of the ball is displaced a geodetic distance m. In (a) we took $a = 1$ and $m = 0.5$; in (b), $a = 8$ and $m = 15$; and in (c), $a = 4$ and $m = 3$. All integrated areas are unitary.

8 General translations

We now generalize the special translations of section 5. We consider a hyperbolic isometry g of H^3 whose axis is ζ, and value t measured along the axis. The solid ball $\mathcal{B}$ with radius a now has centre C at a distance b from the axis; in section 5 we assumed the special value $b = 0$. Under the isometry g the centre C_g of the new ball $\mathcal{B}_g$ is separated m from C; according to (6), we have

$$\sinh(m/2) = \sinh(t/2)\cosh b. \tag{34}$$

We clearly have nonempty intersection $\mathcal{B}\cap\mathcal{B}_g$ only when $m < 2a$; values of the parametres t, b, and a interesting for our purposes then obey the constraint

$$\sinh(t/2)\cosh b < \sinh a. \tag{35}$$

The thickness T, radius R, and volume $V_g^{\mathcal{B}}$ of the solid lens $\mathcal{B}\cap\mathcal{B}_g$ are still given by (12), (13), and (18), with $2M = m(t,b)$ as in (34).

To obtain the probability density $\mathcal{P}_g^{\mathcal{B}}(l)$ we follow the same four steps as described in ref.[3]. The first step is to investigate the shape of the surface $\mathcal{B}\cap\mathcal{C}_r$, where $\mathcal{C}_r$ is the infinitely long cylinder with axis ζ and radius r. The surface $\mathcal{B}\cap\mathcal{C}_r$ is either a topological annulus (if $b + r < a$), or a topological disk (if a, b, and r can form a triangle), or is empty (if $a < |b - r|$). To have the dimensions of $\mathcal{B}\cap\mathcal{C}_r$ we consider a generic point $B = (r, \phi, \zeta)$ of its contour; we note that the distance from B to the centre $C = (b, 0, 0)$ of $\mathcal{B}$ is the radius a, then (11) gives $\zeta(a, b, r, \phi)$ according to

$$\begin{aligned}\cosh a &= \cosh b\cosh r\cosh\zeta \\ &\quad -\sinh b\sinh r\cos\phi;\end{aligned} \tag{36}$$

the variable half width $z(\phi)$ of the intersection is then (eq.(5a) with $e' \to z$ and $g \to \zeta$)

$$z = \zeta\cosh r = \cosh^{-1}(\alpha + \beta\cos\phi)\cosh r, \tag{37}$$

where

$$\alpha = \frac{\cosh a}{\cosh b\cosh r}, \qquad \beta = \tanh b\tanh r. \tag{38}$$

For fixed values of a, b, and r, the intersection $\mathcal{B} \cap \mathcal{C}_r$ lies between the curves $z(\phi)$ and $-z(\phi)$. Figure 12(a) depicts an annulus-like intersection $\mathcal{B} \cap \mathcal{C}_r$, which occurs whenever $0 < r < a - b$ (equivalently $\alpha > \beta + 1$); note that the equator of the annulus measures $2\pi \sinh r$, due to the azimuthal factor $g_{\phi\phi} = \sinh^2 \rho$ in 7. Clearly the extremes $-\pi$ and π of ϕ are identified.

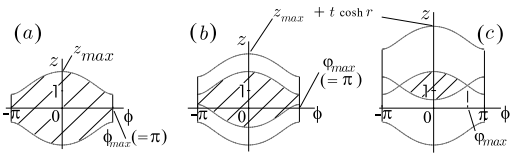

Figure 12 Sample intersections with $a = 2, b = 1$, and $r = 0.9$.
(a) The annulus-like intersection $\mathcal{B} \cap \mathcal{C}_r$.
(b) The (dashed) annulus-like intersection $\mathcal{B} \cap \mathcal{B}_g \cap \mathcal{C}_r$ when $t \cosh r = 1$.
(c) The (dashed) disk-like intersection $\mathcal{B} \cap \mathcal{B}_g \cap \mathcal{C}_r$ when $t \cosh r = 2.5$.

On the other hand, figure 13(a) shows a disk-like intersection $\mathcal{B} \cap \mathcal{C}_r$, which occurs whenever $\alpha < \beta + 1$, with unequal radii z_{max} and $\phi_{max} \sinh r$, with

$$z_{max} = \cosh^{-1}(\alpha + \beta) \cosh r,$$
$$\phi_{max} = \cos^{-1}\left(\frac{1-\alpha}{\beta}\right). \qquad (39)$$

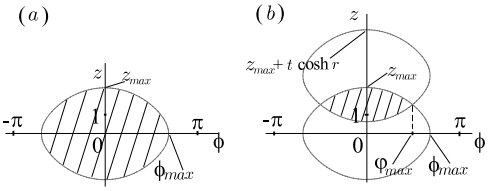

Figure 13 Sample intersections with $a = 2, b = 1$, and $r = 1.2$.
(a) The disk-like intersection $\mathcal{B} \cap \mathcal{C}_r$.
(b) The disk-like intersection $\mathcal{B} \cap \mathcal{B}_g \cap \mathcal{C}_r$ when $t \cosh r = 3$.

The second step is to investigate the shape of the combined intersection $\mathcal{B} \cap \mathcal{B}_g \cap \mathcal{C}_r$. To examine the possible occurrence of annulus-like intersections $\mathcal{B} \cap \mathcal{B}_g \cap \mathcal{C}_r$ we project the centres of $\mathcal{B}$ and $\mathcal{B}_g$ on the ζ axis, and consider the midpoint of these projections; if this midpoint lies inside the solid balls, that is, if $\cosh a > \cosh b \cosh t/2$, then annulus-like intersections $\mathcal{B} \cap \mathcal{B}_g \cap \mathcal{C}_r$ may occur. Otherwise all intersections $\mathcal{B} \cap \mathcal{B}_g \cap \mathcal{C}_r$ are disk-like. Clearly $\mathcal{B} \cap \mathcal{B}_g \cap \mathcal{C}_r$ is the intersection of $\mathcal{B} \cap \mathcal{C}_r$ with $\mathcal{B}_g \cap \mathcal{C}_r$, and $\mathcal{B}_g \cap \mathcal{C}_r$ is an exact copy of $\mathcal{B} \cap \mathcal{C}_r$, only longitudinally displaced a horocyclic distance $t \cosh r$ along $\mathcal{C}_r$. When $\mathcal{B} \cap \mathcal{C}_r$ is annulus-like ($0 < r < a - b$), then $\mathcal{B} \cap \mathcal{B}_g \cap \mathcal{C}_r$ is either annulus-like (when $\cosh(t/2) < \alpha - \beta$, see figure 12($b$), or disk-like (when $\alpha - \beta < \cosh(t/2) < \alpha + \beta$, see figure 12($c$), or is empty (if $\cosh(t/2) > \alpha + \beta$). In the disk-like intersections $\mathcal{B} \cap \mathcal{B}_g \cap \mathcal{C}_r$ the disk extends from $-\varphi_{max}$ to φ_{max}, with (see figures 12(c) and 13(b))

$$\varphi_{max} = \cos^{-1}\left(\frac{\cosh(t/2) - \alpha}{\beta}\right). \qquad (40)$$

When $\mathcal{B} \cap \mathcal{C}_r$ is disk-like, then $\mathcal{B} \cap \mathcal{B}_g \cap \mathcal{C}_r$ is either disk-like (when $\cosh(t/2) < \alpha + \beta$, see figure 13($b$)), or is empty (if $\cosh(t/2) > \alpha + \beta$).

The third step is to evaluate the area $S_g^{\mathcal{B}}(r)$ of the surface $\mathcal{B} \cap \mathcal{B}_g \cap \mathcal{C}_r$. To this end we define the auxiliary function

$$\mathcal{A}(\alpha, \beta, \varphi_{max}) = \int_0^{\varphi_{max}} \cosh^{-1}(\alpha + \beta \cos\phi) d\phi, \qquad (41)$$

in terms of which the areas such as in figures 12(b), 12(c), and 13(b) are

$$S_g^{\mathcal{B}}(r) = [2\mathcal{A}(\alpha, \beta, \varphi_{max}) - t\varphi_{max}] \sinh 2r. \qquad (42)$$

The fourth and last step is to compute

$$\mathcal{P}_g^{\mathcal{B}}(l) = \frac{dr(l)}{dl} \frac{S_g^{\mathcal{B}}[r(l)]}{V_g^{\mathcal{B}}}, \qquad (43)$$

where $r(l)$ is found from (18), and $V_g^{\mathcal{B}}$ from (18) and (34). In figure 14 we reproduce three examples of the density $\mathcal{P}_g^{\mathcal{B}}(l)$ for general hyperbolic translations; clearly all plots start abruptly at $l_{min} \geq t$.

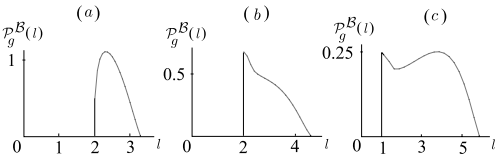

Figure 14 Sample $\mathcal{P}_g^{\mathcal{B}}(l)$ for general translations of H^3; all integrated areas are unitary.
(a) Here $a = 3.5$, $b = 3.1$, and $t = 2$; all intersections $\mathcal{B} \cap \mathcal{C}_r$ and $\mathcal{B} \cap \mathcal{B}_g \cap \mathcal{C}_r$ are disk-like; $l_{min} = t + 0.002$.
(b) Here $a = 3.5$, $b = 2.5$, and $t = 2$; there are disk-like and annulus-like intersections $\mathcal{B} \cap \mathcal{C}_r$, but all $\mathcal{B} \cap \mathcal{B}_g \cap \mathcal{C}_r$ are disk-like; $l_{min} = t$.
(c) Here $a = 3.5$, $b = 2.5$, and $t = 1$; there are both types of intersections of both $\mathcal{B} \cap \mathcal{C}_r$ and $\mathcal{B} \cap \mathcal{B}_g \cap \mathcal{C}_r$; $l_{min} = t$.

9 General screw motions

We already have all elements needed to obtain the probability density $\mathcal{P}_g^{\mathcal{B}}(l)$ of conjugate pair separations for a general screw motion, thus generalizing the results of the preceding sections 5, 6, and 8. We now make use of all four independent parametres, namely

- a = radius of the solid balls $\mathcal{B}$ and $\mathcal{B}_g$,
- b = distance from the centres of the balls to the axis ζ of the isometry,
- t = translation of the isometry, measured along the axis, and
- ω = angle of rotation of the isometry, around the axis.

We shall further write all mathematical expressions in a form appropriate for automatic calculation of $\mathcal{P}_g^{\mathcal{B}}(l)$ in a computer . Without loss of generality for our purposes we assume $t \geq 0$ and $0 \leq \omega \leq \pi$.

The separation $2M$ between the centres of $\mathcal{B}$ and $\mathcal{B}_g$ is now given by (10)

$$\cosh 2M = \cosh^2 b \cosh t - \sinh^2 b \cos\omega, \qquad (44)$$

and the condition $M < a$ is necessary to have nonempty intersection $\mathcal{B}\cap\mathcal{B}_g$. Assuming this condition is fulfilled, the solid lens $\mathcal{B}\cap\mathcal{B}_g$ has thickness T, radius R, and volume $V_g^{\mathcal{B}}$ given by (12), (13), and (18), respectively, with M given by (44). The centre of the lens is at a distance σ from the axis ζ,

$$\tanh\sigma = \frac{\tanh b\cos\omega/2}{\cosh t/2}, \qquad (45)$$

and there always exists one diametre of the lens which is directed perpendicular to the axis ζ. The lens intersects the axis whenever $\sigma < R$, or equivalently $\cosh b\cosh t/2 < \cosh a$.

We next imagine an infinite family of sufficiently long, coaxial (axis ζ), cylindrical surfaces $\mathcal{C}_r$ with variable radius r. We are interested in the intersection of each $\mathcal{C}_r$ with the solid lens $\mathcal{B}\cap\mathcal{B}_g$; clearly only values of r in the range (r_{min}, r_{max}) give nonempty intersections $\mathcal{B}\cap\mathcal{B}_g\cap\mathcal{C}_r$, where

$$r_{min} = (\sigma - R)\,\Theta(\sigma - R)\,, \qquad r_{max} = \sigma + R. \qquad (46)$$

Here Θ is the step function with values 0 and 1. Our strategy to approach $\mathcal{B}\cap\mathcal{B}_g\cap\mathcal{C}_r$ is first study $\mathcal{B}\cap\mathcal{C}_r$, then $\mathcal{B}_g\cap\mathcal{C}_r$, and finally the intersection of these two.

For a given $r\in(r_{min}, r_{max})$ we note that $\mathcal{B}\cap\mathcal{C}_r$ is annulus-like when $r < a-b$, and disk-like otherwise, so we define $\phi_{max} =$

$$\pi\,\Theta(a-b-r) + \cos^{-1}\left(\frac{1-\alpha}{\beta}\right)\Theta(r+b-a)\,, \qquad (47)$$

where $\alpha(a,b,r)$ and $\beta(b,r)$ were given in (38). Each intersection $\mathcal{B}\cap\mathcal{C}_r$ is nonempty for $\phi\in(-\phi_{max},\phi_{max})$, and lies between the two curves

$$z_1 = \cosh^{-1}(\alpha+\beta\cos\phi)\cosh r$$
$$\times\Theta(\phi+\phi_{max})\,\Theta(\phi_{max}-\phi), \qquad z_2 = -z_1\,; \qquad (48)$$

these two curves are drawn on the geometrically flat cylinder $\mathcal{C}_r$.

The intersection $\mathcal{B}_g\cap\mathcal{C}_r$ is identical to $\mathcal{B}\cap\mathcal{C}_r$, but is displaced $t\cosh r$ longitudinally on $\mathcal{C}_r$, and ω azimuthally. It thus lies between the curves

$$z_3 = \tau + \cosh^{-1}\left[\alpha+\beta\cos(\phi-\omega)\right]\cosh r$$
$$\times\Big[\Theta(\phi-\omega+\phi_{max})\,\Theta(\phi_{max}-\phi)$$
$$+\Theta(\phi_{max}-\phi+\omega-2\pi)\,\Theta(\phi+\phi_{max})\Big],$$
$$z_4 = -z_3 + 2\tau, \qquad (49)$$

where

$$\tau = t\cosh r\,\Theta(\phi+\phi_{max})\,\Theta(\phi_{max}-\phi); \qquad (50)$$

the term with the Θ function containing 2π in eq. (49) is included to allow automatic computing.

As in ref.[3], the area $S_g^{\mathcal{B}}(r)$ of the intersection $\mathcal{B}\cap\mathcal{B}_g\cap\mathcal{C}_r$ is

$$S_g^{\mathcal{B}}(r) = \sinh r\int_{-\phi_{max}}^{\phi_{max}}\Theta(z_1-z_4)$$
$$\times\left[\min(z_1,z_3) - \max(z_2,z_4)\right]d\phi. \qquad (51)$$

Finally, the probability density $\mathcal{P}_g^{\mathcal{B}}(l)$ is given by (43) with $r(l)$ coming from (21); we find that

$$\frac{dr}{dl} = \frac{\sinh l\,\mathrm{csch}2r}{\cosh t - \cos\omega}. \qquad (52)$$

In figure 15 a few sample plots of $\mathcal{P}_g^{\mathcal{B}}(l)$ for screw motions in H^3 are given.

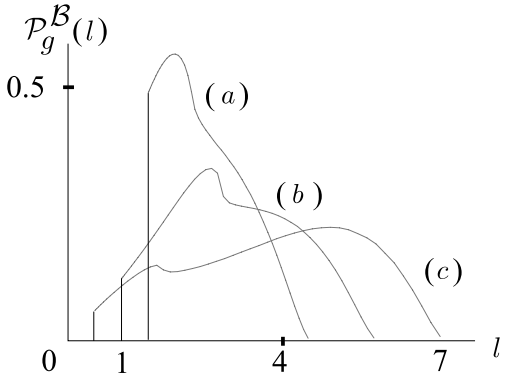

Figure 15 Sample $\mathcal{P}_g^{\mathcal{B}}(l)$ for general screw motions of H^3; all integrated areas are unitary.
(a) Here $a=4$, $b=3$, $t=1.5$, and $\omega=\pi/2$.
(b) Here $a=4$, $b=2.5$, $t=1$, and $\omega=\pi/2$.
(c) Here $a=4$, $b=2.5$, $t=0.5$, and $\omega=\pi/4$.

10 Conclusion

The three plots in figure 15 are the output of a computer program whose inputs are the values of a, b, t, and ω; given these inputs, the program proceeds without any intervention.

The three parametres (t,ω,b) related to the screw motion can be extracted from a 4×4 matrix $\mathcal{M}_g$, which expresses the motion in terms of the minkowskian coordinates $(W;X,Y,Z)$ [4]. Indeed, it can be shown that the trace T, the sum Σ of the principal minors of order 2, and the time-time coefficient U of the matrix $\mathcal{M}_g$ are

$$T = 2(\cosh t + \cos\omega),$$
$$\Sigma = 2(1+2\cosh t\cos\omega),$$
$$U = \cosh t\cosh^2 b - \cos\omega\sinh^2 b; \qquad (53)$$

if we define $V = \sqrt{8+T^2-4\Sigma}$ then we obtain

$$\cosh t = \tfrac{1}{4}(T+V), \quad \cos\omega = \tfrac{1}{4}(T-V),$$
$$\cosh 2b = \frac{4U-T}{V}. \qquad (54)$$

To close this report we show through a concrete example how to use the functions $\mathcal{P}_g^{\mathcal{B}}(l)$ to get information about the topology of the universe. We need first briefly recall the theory that underlies the subject; for details see [2], [5], [6].

Expected (or theoretical) normalized histograms $\phi(i)$ of pair separations are decomposed as

$$\phi(i) = \phi^{un}(i) + \frac{1}{n-1}\sum_g \nu_g \left[\phi^g(i) - \phi^{un}(i)\right], \quad (55)$$

where $\phi^{un}(i)$ is the expected normalized histogram of the uncorrelated pair separations, the i denotes an interval of separations (a bin in the histogram), n is the finite number of objects in the solid ball $\mathcal{B}$, $\nu_g = N_g/n = \nu_{g^{-1}}$ with N_g the number of g-pairs with both members inside $\mathcal{B}$, and $\phi^g(i)$ is the expected normalized histogram of the g-pairs. These $\phi^g(i)$ are the histogramic counterparts of the functions $\mathcal{P}^{\mathcal{B}}_g(l)$ of [3] and of this report. From (55), and accepting a suggestion by Fagundes and Gausmann [7], we write

$$(n-1)[\phi - \phi^{sc}] = (n - 1 - \sum \nu_g)[\phi^{un} - \phi^{sc}] + \sum \nu_g [\phi^g - \phi^{sc}], \quad (56)$$

where $\phi^{sc}(i)$ is the expected normalized histogram of pair separations in a simply connected ball with same radius and geometry as $\mathcal{B}$; it is the histogramic counterpart of the function $\mathcal{F}_H(a,l)$ of [8] and of $\mathcal{F}_H(a,s)$ of [9]. In the limit $n \to \infty$ the products $n[\phi - \phi^{sc}] =: \varphi^{\mathcal{B}}$ and $n[\phi^{un} - \phi^{sc}] =: \varphi^{\mathcal{B}}_{un}$ remain finite, and we write

$$\varphi^{\mathcal{B}}(l) = \varphi^{\mathcal{B}}_{un}(l) + \varphi^{\mathcal{B}}_{\Gamma}(l),$$
$$\varphi^{\mathcal{B}}_{\Gamma}(l) := \sum \nu_g [\mathcal{P}^{\mathcal{B}}_g(l) - \mathcal{P}^{\mathcal{B}}_{sc}(l)]. \quad (57)$$

To go from the various histograms $f(i)$ to the corresponding functions $f(l)$ we have simply made the number of bins tend to infinity. The function $\varphi^{\mathcal{B}}(l)$ has been called the topological signature of a ball $\mathcal{B}$ in a multiply connected space; since in practice the function $\varphi^{\mathcal{B}}_{un}(l)$ is usually small valued when compared with both $\varphi^{\mathcal{B}}(l)$ and $\varphi^{\mathcal{B}}_{\Gamma}(l)$, the function $\varphi^{\mathcal{B}}_{\Gamma}(l)$ is generally a good approximation of the topological signature $\varphi^{\mathcal{B}}(l)$.

We now turn to a specific example: that of a ball $\mathcal{B}$ in the Seifert-Weber dodecahedral space. This multiply connected hyperbolic three-space is obtained from a regular solid dodecahedron $\mathcal{D}$ by pairwise identifying opposite faces using twists of 3/10 of a revolution [10]. We make the centres of $\mathcal{B}$ and $\mathcal{D}$ coincide (a rather uncopernic assumption), and choose $\mathcal{B}$ tangent to the edges of $\mathcal{D}$.

Computer simulations of $(n-1)[\phi(i) - \phi^{sc}(i)]$ for the hyperbolic ball $\mathcal{B}$ are given in the literature (see figure 7 in [6] or figure 3 in [11]), and we now construct its *approximate* expected counterpart $\varphi^{\mathcal{B}}_{\Gamma}(l)$, eq.(57).

We first select two of the 12 matrices of face-pairing isometries of $\mathcal{D}$:

$$\mathcal{M}_1 = \begin{pmatrix} 3.736 & 0 & 0 & 3.600 \\ 0 & -0.309 & -0.951 & 0 \\ 0 & 0.951 & -0.309 & 0 \\ 3.600 & 0 & 0 & 3.736 \end{pmatrix}, \quad (58)$$

$$\mathcal{M}_2 = \begin{pmatrix} 3.736 & -3.220 & 0 & -1.610 \\ -3.220 & 2.927 & 0.425 & 1.618 \\ 0 & -0.425 & -0.309 & 0.851 \\ -1.610 & 1.618 & -0.851 & 0.500 \end{pmatrix}, \quad (59)$$

sufficient for our purposes. Applying (54) to any of $\mathcal{M}_1$ or $\mathcal{M}_2$ we find the values

$$t_1 = 1.992, \quad \omega_1 = 108^o, \quad b_1 = 0, \quad (60)$$

for the translation, the rotation, and the distance from the axis of the isometry to the centre of $\mathcal{B}$ (the origin of coordinates). From (44) and (60) we obtain half separation $M_1 = 0.996$ between the centres of $\mathcal{B}$ and $\mathcal{B}_g$, a value smaller than the radius $a = 1.439$ of $\mathcal{B}$.

We also need consider 60 other isometries, whose common prototype matrix is $\mathcal{M}_3 = \mathcal{M}_1\mathcal{M}_2 =$

$$\begin{pmatrix} 8.163 & -6.205 & -3.062 & -4.215 \\ 0.995 & -0.500 & 0.162 & -1.309 \\ -3.062 & 2.915 & 0.500 & 1.276 \\ 7.434 & -5.545 & -3.178 & -3.927 \end{pmatrix}; \quad (61)$$

each such isometry gives, from (54),

$$t_3 = 1.746, \quad \omega_3 \approx 147^o, \quad b_3 = 0.999. \quad (62)$$

These 60 isometries also contribute to the sum in (57), since from (44) and (62) we find half separation $M_3 = 1.395$, a value smaller than a. All other isometries seem to give $M > a$, so they do not contribute to the sum in (57).

For the 12 fundamental isometries (60) we find intersections $\mathcal{B} \cap \mathcal{B}_g$ with volume $V^{\mathcal{B}}_1 = 1.377$ as given by (18); all produce the same spectrum $\mathcal{P}^{\mathcal{B}}_1(l)$, which has nonzero values only in the interval $l \in (1.99, 2.79)$. On the other hand, for the 60 isometries (62) we find $V^{\mathcal{B}}_3 = 0.011433$, and a spectrum $\mathcal{P}^{\mathcal{B}}_3(l)$ with nonzero values only when $l \in (1.75, 1.99)$. Finally, the probability density $\mathcal{P}^{\mathcal{B}}_{sc}(l)$ for pair separations in a hyperbolic ball is the function $\mathcal{F}_H(a,l)$ of [8], or the function $\mathcal{F}_H(a,s)$ of [9]; for unitary curvature of the space, the volume of the ball with radius $a = 1.439$ is $V^{\mathcal{B}}_{sc} = 18.8$. From (57) we then have (see figure 16)

$$\varphi^{\mathcal{B}}_{\Gamma}(l) = \frac{12V^{\mathcal{B}}_1}{V^{\mathcal{B}}_{sc}}\left[\mathcal{P}^{\mathcal{B}}_1(l) - \mathcal{P}^{\mathcal{B}}_{sc}(l)\right] + \frac{60V^{\mathcal{B}}_3}{V^{\mathcal{B}}_{sc}}\left[\mathcal{P}^{\mathcal{B}}_3(l) - \mathcal{P}^{\mathcal{B}}_{sc}(l)\right]. \quad (63)$$

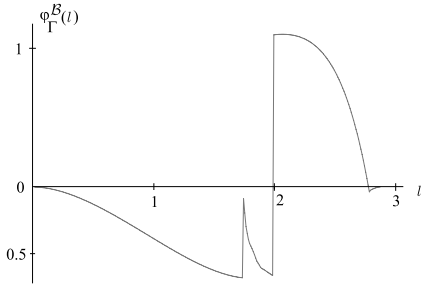

Figure 16 Approximate topological signature $\varphi^{\mathcal{B}}_{\Gamma}(l)$ for an observed universe endowed with the Seifert-Weber dodecahedral topology and unitary negative curvature. The centre of observation and that of the dodecahedron coincide, and the event horizon is supposed $a = 1.44$ away. The discontinuities observed at $l = 1.75$ and $l = 1.99$ derive from isometries, as described in the text. Their localization and strength are good indicators of the topology of the universe.

The approximate signature $\varphi_{\Gamma}^{\mathcal{B}}(l)$ of figure 16 bears close similarity with the corresponding histograms figure 7 in [6] and figure 3 in [11]. However, some small distortion can be seen, probably arising because the uncorrelated contribution $\varphi_{un}^{\mathcal{B}}(l)$, present in (57), was not taken into account. As a matter of fact, we have not been able to obtain the expected $\varphi_{un}^{\mathcal{B}}(l)$ neither for the present Seifert-Weber space nor for any simpler $3D$ nontrivial manifold, such as the three-torus. Even for the two-torus that function has been eluding our efforts; only for the one-torus (a circle) we have already succeeded in finding the $\varphi_{un}^{\mathcal{B}}(l)$ [12].

Acknowledgments

The author is grateful to A. Bernui, G.I. Gomero and M.J. Rebouças for fruitful conversations.

References

[1] R. Lehoucq, M. Lachièze-Rey, and J.-P. Luminet, *Cosmic crystallography*, Astron. Astroph. **313**, 339-346 (1996); http://www/ arxiv.org/ abs/ gr-qc/9604050.

[2] G.I. Gomero, A.F.F. Teixeira, M.J. Rebouças and A. Bernui, *Spikes in cosmic crystallography*, gr-qc/9811038, version 3.

[3] A. Bernui and A.F.F. Teixeira, *Cosmic crystallography: the euclidean isometries*, gr-qc/0003063.

[4] J.R.Weeks, *SnapPea: a computer program for creating and studying hyperbolic manifolds*, available from the Web site www.northnet.org/weeks.

[5] G.I. Gomero, M.J. Rebouças and A.F.F. Teixeira, *Spikes in cosmic crystallography II: topological signature of compact flat universes*, gr-qc/9909078 , to appear in *Phys. Letters A* (2000).

[6] G.I. Gomero, M.J. Rebouças and A.F.F. Teixeira, *A topological signature in cosmic topology*, gr-qc/9911049.

[7] H.V. Fagundes and E. Gausmann, *Cosmic crystallography in compact hyperbolic spaces*, astro-ph/9811368.

[8] A. Bernui and A.F.F. Teixeira, *Cosmic crystallography: three multipurpose functions*, astro-ph/9904180.

[9] M.J. Rebouças, *Distinguishing marks of simply connected universes*, gr-qc/0007040, to appear in *Int. J. Mod. Phys. D* (2000).

[10] J.R. Weeks, *The shape of space*. Marcel Dekker, Inc., New York, 1985. Also W.P. Thurston, *Three-Dimensional Geometry and Topology, vol. 1*, edited by Silvio Levy. Princeton Univ. Press, Princeton, 1997.

[11] G.I. Gomero, M.J. Rebouças and A.F.F. Teixeira, *Signature for the shape of the universe*, to appear in *Int. J. Mod. Phys. D* (2000).

[12] A.F.F. Teixeira, *Cosmic crystallography in a circle*, gr-qc/0005052 .